HEAT TRANSFER- ASIAN RESEARCH

Online ISSN:1523-1496; Publisher – Wiley (NEW YORK, USA).

Accepted January 20TH 2019

NUMERICAL COMPUTATION OF NON-LINEAR OSCILLATORY TWO-IMMISCIBLE MAGNETOHYDRODYNAMIC FLOW IN DUAL POROUS MEDIA SYSTEM: FTCS AND FEM STUDY

O. Anwar Bég[a], A. Zaman[b], N. Ali[b], S.A. Gaffar[c*] and Tasveer A. Bég[d]

[a] Magnetohydrodynamics, Biological Propulsion and Energy Research, Aeronautical and Mechanical Engineering Department, Newton Building, University of Salford, M5 4WT, UK.

[b] Fluid Mechanics Group, Dept. Mathematics & Statistics, Int. Islamic Univ., Islamabad 44000, Pakistan.

[c] Dept. Mathematics, Salalah College of Technological, Salalah, Oman

[d] Renewable Energy/Geodynamics Research, Israfil House, Dickenson Road, Manchester, M13, England, UK.

Corresponding Author; Email: abdulsgaffar0905@gmail.com

Abstract

The transient Hartmann magnetohydrodynamic (MHD) flow of two immiscible fluids flowing through a horizontal channel containing two porous media with oscillating lateral wall mass flux is studied. A two-dimensional spatial model is developed for the two fluids, one of which is electrically-conducting and the other electrically-insulating (as is the wall in the second region). Both fluid regimes are driven by a common pressure gradient. A Darcy-Forchheimer drag force model is used to simulate the porous medium effects on the flow in both fluid regions. Special boundary conditions are imposed at the interface. The governing second order nonlinear partial differential equations are non-dimensionalized for each region using a set of transformations. The resulting transport equations are shown to be controlled by the Hartmann hydromagnetic parameter (Ha), viscosity ratio parameter (α), two Darcy numbers (Da_1, Da_2), two Forchheimer numbers (Fs_1, Fs_2), two Reynolds numbers (Re_1, Re_2), frequency parameter (εA) associated with the transpiration (lateral wall flux) velocity and a periodic frequency parameter (ω^*t^*). Numerical FTCS finite difference solutions are obtained for a wide range of the governing parameters. Benchmarking is performed with a Galerkin finite element method code (MAGNETO-FEM) and the results are found to be in excellent agreement. Applications of the model include magnetic cleanup operations in coastal/ocean seabed oil spills and electromagnetic purification of petroleum reservoir fluids.

Key words: *Electromagnetic flow; environmental electrical engineering, Immiscible; porous; FTCS; FEM; oil spill hazard; magnetic clean up; Hartmann number; electrical conductivity; frequency*.

1. Introduction

Multi-fluid transport is an area of great interest in various branches of engineering and geophysical sciences. In petroleum recovery, stratified two-liquid flows are commonly encountered. Packam and Shail [1] presented an early study of stratified laminar hydrodynamics of two immiscible fluids in a horizontal conduit. Ranger [2] studied the two-phase flow of two immiscible fluids in a diverging channel. Napolitano [3]

investigated the plane Poiseuille flow of two immiscible fluids in a non-isothermal capillary channel under combined surface tension, gravitational and pressure gradient effects using an analytical approach. The stability of plane Poiseuille flow of two immiscible fluids with differing viscosities was studied in channels by Than *et al.* [4]. In these investigations the fluids were assumed to be non-conducting. However many applications exist in which *magnetohydrodynamic two-fluid flows* arise, for example in the liquid metal magnetofluid dynamic power generators, control of oil flows in pipelines, desalination systems, liquid stirring tanks, plasma flow control devices etc. This has stimulated some interest in the analysis of two-fluid immiscible flows in the presence of a transverse magnetic field with or without simultaneous heat transfer. Khedr *et al*. [5] explored the MHD flow of a micropolar fluid along a vertical semi-infinite permeable plate in the presence of wall suction or injection and heat generation or absorption effects. Chamkha [6] investigated the MHD free convection flows along a vertical plate embedded in a thermally stratified porous medium. Magyari and Chamkha [7] presented the exact solutions of MHD thermosolutal Marangoni convection flows due to imposed temperature and concentration in the presence of constant magnetic field. Chamkha and Mudhaf [8] used implicit, iterative finite-difference scheme to study the unsteady mixed convection flow over a vertical permeable rotating cone in the presence of magnetic field and heat generation or absorption effects. Chamkha and Khaled [9] considered the mixed convection in a stagnation flow over a flat plate embedded in porous medium. Chamkha [10] studied the closed-form transient solutions for hydromagnetic two-phase particulate suspension flow in channels and circular pipes. Shail [11] presented one of the earliest studies of the Hartmann flow of a conducting fluid in a channel between two horizontal infinite plates (both insulating) comprising a layer of non-conducting fluid between the conducting liquid and upper channel wall. Using a volumetric flow rate factor it was shown that considerable enhancement in the conducting fluid flow rate can be achieved for appropriate depth and viscosity ratios of the two fluids. More recently Baier and Graham [12] studied the *two-fluid Taylor-Couette flow* i.e. centrifugal instability of two radially stratified immiscible fluids in the annular gap between co-rotating cylinders. Their experiments showed that for fluids of sufficiently small viscosity a new instability is present in the two-fluid system which is similar to that of a thin film of liquid coating the

interior of a rotating drum. These studies have considered homogenous fluid continua. In many geophysical applications however, porous media are also of great importance. Transport in such domains can be modeled in a variety of ways including spatially-periodic models [13], volume-averaging procedures [14] and drag-force models [15]. The conventional model for slow, viscous flows in porous media is the Darcian model which simulates bulk porous media effects associated with pressure drop. At higher velocities a *non-linear* model is needed and the popular approach is to employ the Forchheimer-extended-Darcy model. Bég and co-workers [16-23] have utilized the Darcy-Forchheimer porous model (and also the Darcian model) in numerous magnetofluid porous media transport phenomena problems including biomagnetic rheological blood flow in tissue structures [16], magneto-convection from a sphere in porous media [17], transient viscoelastic boundary layers in Darcy-Brinkman-Forchheimer porous materials [18], magneto-micropolar blood filtration [19], pulsatile blood flow and pharmacological dispersion control [20], radiative magnetized polymer flows [21], magnetic nano-convection [22] and rotating conducting flows in permeable systems. These studies were nevertheless confined to *single liquid flows* in porous media. Two-fluid flows in porous media, although equally important, for example in geothermal energy systems, oil recovery and planetary magnetohydrodynamics, have received less consideration. Several excellent articles have however been communicated. Lennon [24] employed boundary element procedures to analyze the three-dimensional, two-fluid hydraulics in porous media. DeGregoria [25] studied the two-fluid flow in porous media at finite viscosity ratio based on Monte Carlo simulations. Both linear channel and more complex geometries were examined at various numerical grid sizes. Casulli and Greenspan [26] numerically studied the hydrodynamics of miscible and immiscible fluid transport in geomaterials with applications in enhanced petroleum recovery. Than *et al*. [27] reported on Lattice-Boltzmann computations of the two-fluid ideal flow in porous media, at the pore scale. They studied the specific case of water and tetrachloroethylene in a glass-bead porous system. Chamkha [28] examined steady, laminar magneto-heat transfer in two viscous, heat generating/absorbing fluids in a porous medium channel with applications in magnetohydrodynamic coal-fired generators.

Newly developed technologies in de-contamination of crude oil accidents in coastal zones penetrating into sea beds have garnered some interest. These magneto-hydrodynamic oil spill control methods exploit the electrically-conducting nature of ocean water (seawater) and magnetic fields have been shown to quickly separate oil from ecosystems, using the electromagnetic Lorentz force which characterizes magnetohydrodynamics [29]. This approach minimizes environmental impact and is portable and very adaptive. In the present study, motivated by such applications in environmental petroleum engineering, we consider the hydrodynamics of two immiscible fluids in a *dual porous medium* system with oscillatory wall suction. One fluid is electrically-conducting and the other electrically-insulating. The fully-developed, laminar unsteady flow equations are presented, non-dimensionalized and solved using a numerical method (finite differences). Computations are validated with a Galerkin finite element method. The effects of the control parameters, viz *Darcy number, Forchheimer number, fluid viscosity ratio, Hartmann number and Reynolds number* are studied in detail. Such a study has thusfar not been reported in the literature. The present 2-dimensional simulations should also serve as a good benchmark for more complex 3-D models using commercial codes.

2. Mathematical Model

Consider the transient, incompressible, fully-developed flow of a Newtonian two-fluid electromagnetic system through a parallel-plate channel configuration containing homogenous, isotropic porous media. The physical regime is shown in **figure 1** below. The plates are infinitely long and orientated along the x and z coordinates i.e. they lie in the xz-plane. The y-coordinate is normal to the longitudinal axes of the plates. In region A ($0 \leq \leq$) , the fluid is electrically-conducting, possessing a dynamic viscosity μ_1 and mass density ρ_1. This region contains a porous medium of permeability K_1 and a Forchheimer inertial geometric parameter, b_1. Region B contains electrically non-conducting fluid with dynamic viscosity μ_2, mass density ρ_2, flowing through a porous medium of permeability K_2 and a Forchheimer inertial geometric parameter, b_2. Transverse to the flow direction a constant strength magnetic field, B_o, is applied. Induced magnetic field effects are neglected as the magnetic Reynolds number is small for weak magnetic fields. All fluid and porous media properties are constant for each region. Thermoelectric and electro-hydrodynamic effects

and porous medium deformability are all neglected. In addition both fluids are assumed to *fully saturate* each region. A common pressure gradient, $-\frac{\partial p}{\partial x}$, drives the flow in both regions. The governing equations driving the flow can then be shown to reduce from the Navier-Stokes equations to the following form, with hydromagnetic body force term in Region A and both Darcian porous bulk drag and Forchheimer inertial (second order) drag in Regions A and B:

Region A:

Mass Conservation

$$\frac{\partial v_1}{\partial y} = 0 \tag{1}$$

Momentum Conservation:

$$\rho_1[\frac{\partial u_1}{\partial t} + v_1 \frac{\partial u_1}{\partial y}] = \mu_1 \frac{\partial^2 u_1}{\partial y^2} - \frac{\partial p}{\partial x} - \sigma_1 u_1 B_o{}^2 - \frac{\nu_1}{K_1} u_1 - \frac{b_1}{K_1} u_1{}^2 \tag{2}$$

Region B:

Mass Conservation

$$\frac{\partial v_2}{\partial y} = 0 \tag{3}$$

Momentum Conservation:

$$\rho_2[\frac{\partial u_2}{\partial t} + v_2 \frac{\partial u_2}{\partial y}] = \mu_2 \frac{\partial^2 u_2}{\partial y^2} - \frac{\partial p}{\partial x} - \frac{\nu_2}{K_2} u_2 - \frac{b_2}{K_2} u_2{}^2 \tag{4}$$

where u is the x-direction fluid velocity, v is the y-direction fluid velocity, t denotes time and σ is the electrical conductivity. The subscripts $( )_1$ and $( )_2$, are associated with Region A and Region B respectively. No-slip velocity boundary conditions are imposed so that the x-velocity component is zero at the plates. Following Loharsbi and Sahai [30] there is *continuity of velocity and shear stress at the interface* between the two fluid layers i.e. at y = 0. The penultimate and final terms on the right hand side of equations (2) and (4) designate the Darcian linear porous drag and Forchheimer quadratic drag in each region, respectively. The corresponding plate boundary and *interfacial* conditions for the effectively fourth order decoupled system of partial differential equations for the flow regime are:

$$u_1(h) = 0,\ u_2(-h) = 0,\ u_1(0) = u_2(0),\ \mu_1 \frac{\partial u_1}{\partial y} = \mu_2 \frac{\partial u_2}{\partial y} \ \text{ at } \ y = 0 \qquad (5)$$

From the mass conservation equations (1) and (3) the y-direction velocity components in each region, viz v_1 and v_2, are independent of y-coordinate. They are assumed to be a harmonic function of time only, and denoting $v = v_1 = v_2$, following Umavathi *et al*. [31], we define:

$$v = v_o[1 + \varepsilon A^{i\omega t}] \qquad (6)$$

where A is a real positive constant, ε is a small value constant obeying the condition $\varepsilon A \leq 1$, and ω is the frequency of the oscillatory motion. In the present analysis, therefore wall *transpiration* is present (lateral mass flux) which is defined by a velocity, v, that varies periodically with time about a non-zero mean, v_o. For the special case of $\varepsilon A = 0$, constant (non-oscillatory) wall transpiration is recovered. The present boundary value problem is well-posed and can be solved by a variety of numerical methods. However such solutions would be based on a single geometrical configuration and could not be scaled to any possible system arising in industrial technologies. We therefore implement a *non-dimensionalization* procedure by introducing a set of dimensionless parameters to convert the present problem into a generalized one, independent of dimensions and applicable to any size of parallel plate two-fluid system. Defining the following change of variables:

$$u_1 = \bar{u}_1 u_1^*,\ y = hy^*,\ t = \frac{h^2}{\nu} t^*.\ \ v = \frac{\nu}{h} v^*,\ \omega = \frac{\nu}{h^2}\omega^*,\ p^* = \frac{h^2}{\mu_1 \bar{u}_1}\left[\frac{\partial p}{\partial x}\right],$$

$$Da_1 = \frac{K_1}{h^2},\ Da_2 = \frac{K_2}{h^2},\ Fs_1 = \frac{b_1}{h},\ Fs_2 = \frac{b_2}{h},\ Ha = B_o h\sqrt{\frac{\sigma_1}{\mu_1}},\ \mathrm{Re}_1 = \frac{hu_1}{\nu_1},$$

$$\mathrm{Re}_2 = \frac{hu_2}{\nu_2},\ \alpha = \frac{\mu_2}{\mu_1}. \qquad (7)$$

where u_1^* is dimensionless velocity in x-direction in region A, y^* is dimensionless coordinate normal to the plane of the plates, t^* is the dimensionless time parameter, v^* is dimensionless y^*-direction velocity in both regions A and B, ω^* is dimensionless frequency parameter, p^* is dimensionless pressure, Da_1, Fs_1, Re_1 are the Darcy number, Forchheimer inertial (quadratic drag) number and Reynolds number for region A, Da_2, Fs_2, Re_2 are the Darcy number, Forchheimer number and Reynolds number for region B and Ha is the Hartmann hydromagnetic number for region A only. The parameter α denotes the ratio of the fluid viscosities. The dimensionless two-fluid momenta equations are thereby reduced for region A and region B, respectively to:

$$\frac{\partial u_1^*}{\partial t^*} + v^*\frac{\partial u_1^*}{\partial y^*} = p^* + \frac{\partial^2 u_1^*}{\partial y^{*2}} - Ha^2 u_1^* - \frac{u_1^*}{Da_1} - \frac{Fs_1\,\mathrm{Re}_1}{Da_1}u_1^{*2} \qquad (8)$$

$$\frac{\partial u_2^*}{\partial t^*} + v^*\frac{\partial u_2^*}{\partial y^*} = p^* + \alpha\frac{\partial^2 u_2^*}{\partial y^{*2}} - \frac{u_2^*}{Da_2} - \frac{Fs_2\,\mathrm{Re}_2}{Da_2}u_2^{*2} \qquad (9)$$

The dimensionless hydrodynamic boundary and interfacial conditions for the two fluids are found to be:

$$u_1^*(1) = 0,\ u_2^*(-1) = 0,\ u_1^*(0) = u_2^*(0),\ \frac{\partial u_1^*}{\partial y^*} = \alpha\frac{\partial u_2^*}{\partial y^*}\ \ at\ \ y^* = 0 \qquad (10)$$

3. Special Cases

Let us briefly study now some special cases of the generalized mathematical model. Several of these have been presented in order to provide comparison solutions with an alternative numerical method (FEM).

Case I: Oscillatory Hartmann Flow in a Two-Fluid Two-Darcian Porous Medium

Setting $Fs_1 = 0$ *and* $Fs_2 = 0$ in equations (8) and (9), we arrive at the Darcian flow case for each region A and B, viz:

$$\frac{\partial u_1^*}{\partial t^*} + v^* \frac{\partial u_1^*}{\partial y^*} = p^* + \frac{\partial^2 u_1^*}{\partial y^{*2}} - Ha^2 u_1^* - \frac{u_1^*}{Da_1} \tag{11}$$

$$\frac{\partial u_2^*}{\partial t^*} + v^* \frac{\partial u_2^*}{\partial y^*} = p^* + \alpha \frac{\partial^2 u_2^*}{\partial y^{*2}} - \frac{u_2^*}{Da_2} \tag{12}$$

Case II: Oscillatory Hartmann Flow in a Two-Fluid Medium

Prescribing $Da_1 \to \infty$ *and* $Da_2 \to \infty$ in equations (8) and (9), the porous media in the limit vanish and the regions A and B become purely fluid regimes. Case I can be further contracted therefore to produce the momenta equations used by Umavathi *et al.* [31] (in that study however heat transfer was also considered):

$$\frac{\partial u_1^*}{\partial t^*} + v^* \frac{\partial u_1^*}{\partial y^*} = p^* + \frac{\partial^2 u_1^*}{\partial y^{*2}} - Ha^2 u_1^* \tag{13}$$

$$\frac{\partial u_2^*}{\partial t^*} + v^* \frac{\partial u_2^*}{\partial y^*} = p^* + \alpha \frac{\partial^2 u_2^*}{\partial y^{*2}} \tag{14}$$

Case III: Oscillatory Flow in a Two-Fluid Medium

Setting $Ha \to 0$ in equation (13) negates all magnetohydrodynamic effects and region A is now also electrically non-conducting, as region B. Case II is therefore simplified only via (13) to give:

$$\frac{\partial u_1^*}{\partial t^*} + v^* \frac{\partial u_1^*}{\partial y^*} = p^* + \frac{\partial^2 u_1^*}{\partial y^{*2}} - Ha^2 u_1^* \tag{15}$$

Case IV: Oscillatory Hartmann Flow in a Two-Fluid Single Darcy-Forchheimer Porous Medium

With $Da_1=Da_2$ *and* $Fs_1=Fs_2$, the porous media in regions A and B become identical. This case is important when immiscible fluids are flowing in the same porous body e.g. geomaterial. Using a single Darcy number, *Da* and single Forchheimer number, *Fs*, the general equations (8) and (9) reduce then to:

$$\frac{\partial u_1^*}{\partial t^*} + v^* \frac{\partial u_1^*}{\partial y^*} = p^* + \frac{\partial^2 u_1^*}{\partial y^{*2}} - Ha^2 u_1^* - \frac{u_1^*}{Da} - \frac{Fs\,\mathrm{Re}_1}{Da} u_1^{*2} \tag{16}$$

$$\frac{\partial u_2^*}{\partial t^*} + v^* \frac{\partial u_2^*}{\partial y^*} = p^* + \alpha \frac{\partial^2 u_2^*}{\partial y^{*2}} - \frac{u_2^*}{Da} - \frac{Fs\,\mathrm{Re}_2}{Da} u_2^{*2} \tag{17}$$

We note that as the fluid viscosities are still different, two Reynolds numbers are still required to accurately represent the hydrodynamic problem.

Case V: Steady Hartmann Flow in a Two-Fluid Two-Darcian Porous Medium

Case I may be converted to the steady-state case by negating the velocity gradients i.e. temporal terms in equations (21) and (22). In addition the transpiration velocity will now be constant ($v = v_o$ in equation (6)) as $\varepsilon A \to 0$ for the steady state scenario. The steady flow equations will then become:

$$v^* \frac{\partial u_1^*}{\partial y^*} = p^* + \frac{\partial^2 u_1^*}{\partial y^{*2}} - Ha^2 u_1^* - \frac{u_1^*}{Da_1} \tag{18}$$

$$v^* \frac{\partial u_2^*}{\partial y^*} = p^* + \alpha \frac{\partial^2 u_2^*}{\partial y^{*2}} - \frac{u_2^*}{Da_2} \tag{19}$$

Case VI: Steady Hartmann Flow in a Two-Fluid Medium

Case V can now be reduced to steady-state magnetohydrodynamic flow in a purely two-immiscible fluid medium by once again setting $\mathrm{Da}_1 \to \infty$ and $\mathrm{Da}_2 \to \infty$. Equations (18) and (19) will then become:

$$v^* \frac{\partial u_1^*}{\partial y^*} = p^* + \frac{\partial^2 u_1^*}{\partial y^{*2}} - Ha^2 u_1^* \tag{20}$$

$$v^* \frac{\partial u_2{}^*}{\partial y^*} = p^* + \alpha \frac{\partial^2 u_2{}^*}{\partial y^{*2}} \tag{21}$$

Case VII: Steady Flow in a Two-Fluid Medium

Finally Case VI can further be reduced to *non-electrically conducting* flow in both regions A and B by setting *Ha* = 0 for region A. Of course as with case III, only the Lorentz hydromagnetic body force term will be affected in equation (20) which will reduce to:

$$v^* \frac{\partial u_1{}^*}{\partial y^*} = p^* + \frac{\partial^2 u_1{}^*}{\partial y^{*2}} \tag{22}$$

The region-B momentum equation will remain the same as for case VI.

We note that in all the steady state cases, *p* i.e. dimensionless pressure gradient is not affected as this is a steady gradient driving the flow. Unsteadiness is only experienced via the time-dependent velocity gradients and the *y**-direction velocity component, *v**, which as discussed above loses harmonic properties for the steady state case. Finally it is pertinent to mention that while the Hartmann number does not arise in the region B momentum equation, it is expected to indirectly affect the velocity field in region B via coupling with the v* velocity in the momentum equation for region A. Of course the influence of *Ha* will be more pronounced on velocity development in region A.

4. FTCS Numerical Solution

Explicit finite difference methods are commonly used for the solution of parabolic partial differential equations. The nonlinear differential system for the present flow (Eqns. (8-10)) is also parabolic in nature. Therefore, its solution can be readily found by explicit finite difference formulation. The forward time/central space (FTCS) method, Richardson method and DuFort-Frankel method are the available explicit finite difference schemes. It is just a matter of choice to use any one of them. The present problem is solved using the FTCS method. This method has been recently employed by Ali *et al.* [32]. For more details of this method regarding convergence and stability, the reader is referred to the book by Hoffmann and Chiang (section 3.3 page 64) [33]. For a general variable, *w*, according to this scheme the various partial derivatives of *w* appearing in (8) and (9) are approximated as follows in space (*x*) and time (*t*) coordinates:

$$\frac{\partial w}{\partial x} \cong \frac{w_{i+1}^{k} - w_{i-1}^{k}}{2\Delta x} = w_x, \tag{23}$$

$$\frac{\partial^2 w}{\partial x^2} \cong \frac{w_{i+1}^{k} - 2w_{i}^{k} + w_{i-1}^{k}}{\left(\Delta x\right)^2} = w_{xx}, \tag{24}$$

$$\frac{\partial w}{\partial t} \cong \frac{w_{i}^{k+1} - w_{i}^{k}}{\Delta t}. \tag{25}$$

where w_i^k denotes the value of w at node x_i and at time instant t_k. In the present simulations we conducted grid independence and also time-independence tests and experimented with different space steps and time steps. The prescribed tolerance for computations was specified as 10−7 i.e. for both the space and time stepping, when the absolute difference between the corresponding numerical values is less than the prescribed tolerance, then it can be inferred that the results are accurate up to seven decimal places for Δt and Δx. For the present problem, an accuracy of 10^{-7} is achieved by taking Δt = 0.00001 and Δx = 0.025. Smaller values of these steps merely achieve the same accuracy but require significantly longer computational times. At a particular location in the solution domain (finite difference grid), the simulations are carried out for a specific value of the temporal and spatial step sizes, $\Delta t = \Delta t_1$ and $\Delta x = \Delta x_1$. Indeed, it is anticipated that for this specific choice, the numerical values of velocity may not be convergent. This claim can be verified by choosing lower values of $\Delta t = \Delta t_2(\Delta t_1)$ and $\Delta x = \Delta x_1(\Delta x_2)$, and then comparing the numerical values of velocity with the previously obtained values. This approach is generally quite efficient and further elaboration is given by Hoffmann and Chiang [33]. Further details for other nonlinear multi-physical problems are documented in the articles [34]-[38]"

5. Galerkin FEM Validation

The explicit numerical scheme has been validated using a Galerkin finite element method (**FEM**). This approach has been used extensively in recent years in transient and magnetohydrodynamic (MHD) flows. Gupta *et al*. [39] studied non-Newtonian heat

transfer from an extending polymer sheet at high temperature with FEM. Other applications which have successfully simulated complex nonlinear flow problems with FEM algorithms include smart biomagnetic tribology [40], rotating magnetized nanofluid dynamics [41], double-diffusive unsteady rheological flow [42] and chemically reacting magneto-convection [38]. FEM uses the opposite approach to FDM, viz numerical integration rather than numerical differentiation. Dropping the * notation and applying the Galerkin finite element method to equations (8) to (9) over the element (e) ($y_j \leq y \leq y_k$), we have [39-45]:

$$\int_{y_j}^{y_k} N^{(e)^T} \left(\frac{\partial u_1^{(e)}}{\partial t} + v \frac{\partial u_1^{(e)}}{\partial y} - p - \frac{\partial^2 u_1^{(e)}}{\partial y^2} + Ha^2 u_1^{(e)} + \frac{u_1^{(e)}}{Da_1} + \frac{Fs_1 \operatorname{Re}_1}{Da_1} u_1^{(e)2} \right) dy = 0 \tag{26}$$

$$\int_{y_j}^{y_k} N^{(e)^T} \left(\frac{\partial u_2^{(e)}}{\partial t} + v \frac{\partial u_2^{(e)}}{\partial y} - p^{(e)} - \alpha \frac{\partial^2 u_2^{(e)}}{\partial y^2} + \frac{u_2^{(e)}}{Da_2} + \frac{Fs_2 \operatorname{Re}_2}{Da_2} u_2^{2(e)} \right) dy \tag{27}$$

We postulate *linear piecewise approximate* solutions for the velocity components as follows:

$$\begin{cases} u_1^{(e)} = N_j(y) u_{1j}(t) + N_k(y) u_{1k}(t) = N_j u_{1j} + N_k u_{1k} \\ u_2^{(e)} = N_j(y) u_{2j}(t) + N_k(y) u_{2k}(t) = N_j u_{2j} + N_k u_{2k} \end{cases} \tag{28}$$

Here:

$$\begin{cases} N_j = \dfrac{y_k - y}{y_k - y_j} \\ N_k = \dfrac{y - y_j}{y_k - y_j} \\ N^{(e)^T} = [N_j N_k]^T = \begin{bmatrix} N_j \\ N_k \end{bmatrix} \end{cases} \tag{29}$$

Here $N_{j,k}$ are the shape functions (interpolation functions). In order to prove the convergence and stability of the Galerkin finite element method, the **Matlab** program **MAGNETO-FEM** is executed with slightly modified values of the mesh distance in the *y-and t-directions i.e.* ***j*** *and* ***k,*** and no significant change is observed in the values of the velocity components. Mesh independence of solutions was therefore achieved with

excellent stability and convergence [45]. The boundary conditions (10) are easily specified in **MAGNETO-FEM**. To validate the **FTCS** finite difference code, a comparison solution is performed for the case $Da = Da_1 = Da_2 = 0.1$, $Fs = Fs_1 = Fs_2 = 0.1$, $Re_1 = Re_2 = 5$, $Ha = 2$, $p = 5.0$, $\omega^* t^* = 2.36$, $\omega^* = 0.75$, $A = 0.1$. *In this case both velocity components are identical.* We have tabulated *y (-1 to 1) versus u i.e.* $u_1^* = u_2^*$ *(region A =region B)* for various α variation (equivalent viscosity case i.e. only one fluid viscosity) below in **Table 1**. For all cases of the viscosity, excellent correlation is achieved between **FTCS** difference scheme and Galerkin **MAGNETO-FEM**. The porous medium is discretized into a domain which is delineated into smaller elements (sub-domains) of finite dimensions called "finite elements". The collection of elements is called *the finite-element mesh* or grid. The element matrix, which is called a *stiffness matrix*, is constructed by using *element interpolation functions*. The algebraic equations so obtained are assembled by imposing the inter-element continuity conditions. This yields a large number of algebraic equations defining the *global finite element model*, which governs the whole domain. The essential and natural boundary conditions are imposed on the assembled equations. The assembled equations so obtained can be solved by any "matrix" numerical technique e.g. Householder's approach, LU Decomposition method etc. Further details are readily available in [39-45]. Criteria for the selection for elements are also documented in the extensive review by Bég [45]. The non-linear algebraic system of equations is solved iteratively. An accuracy of 0.00001 is used. A convergence criterion based on the relative difference between the current and previous iterations is employed. When these differences reach the desired accuracy, the solution is assumed to have converged and the iterative process is terminated. Two-point Gaussian quadrature is implemented for solving the integrations. The FEM algorithm has been executed in **MATLAB** running on an Octane SGI desktop workstation and takes 15-20 seconds on average. Excellent correlation is obtained in **Table 1** between **MAGNETO-FEM** and the **FTCS**, testifying to the validity of the latter computations, which are used in all graphical illustrations. Confidence in the **FTCS** code is therefore high.

6. Numerical Computations and Discussion

The nonlinear boundary value problem defined by eqns. (8) and (9) under boundary conditions (10) is controlled by a number of physical parameters, viz *Ha [Hartmann hydromagnetic number for region A only]*, *εA (transpiration frequency parameter) [which controls v*]*, v_o *(transpiration velocity), p* (dimensionless pressure gradient), Da_1, Da_2 [Darcy numbers for region A and region B], Fs_1, Fs_2 [Forchheimer numbers for region A and B] Re_1 and Re_2 [Reynolds numbers for region A and B]*, α *[ratio of the fluid viscosities of the two regions]*.In the FTCS finite difference numerical computations, default values of parameters are assumed thus: *Ha = 2, εA = 0.1 (A = 0.1), ω*t* = 2.36, p = 5.0, Da_1,= 0.1, Da_2 = 0.1, Fs_1, = 0.1 Fs_2 = 0.1 Re_1 = Re_2 =5,* $v_0 = 2$, *α = 1.0, ω* = 0.75* [i.e. the default values are for non-Darcian hydromagnetic case and assume that both regions A and B are the same porous medium and both fluids have the same viscosity and therefore Reynolds number]. The dual velocity distributions are plotted in **figs. 2-11**.

Figure 2 illustrates the influence of the Hartmann number, *Ha* on the velocity fields. It is immediately apparent that at the juncture of the two porous media i.e. the line y = 0, a smooth progression from region A to region B is achieved. The boundary condition at the interface is therefore physically sensible and also achieves the gradual transition required. With increasing Hartmann number, there is an evident suppression in the velocities through both regions. The geometry of profiles is also altered significantly from parabolic distributions at low Hartmann number to skewed asymmetric distributions at higher Hartmann number. The application of a transverse magnetic field normal to the flow direction has a tendency to induce undulating behaviour at high Hartmann number. The appearance of a point of inflection mid-way across region A at high Hartmann number has also been identified for the purely fluid case by Umavathi *et al.* [31], although they considered heat transfer also. This disturbance in the normally parabolic profiles is induced by stronger magnetic field, and is more pronounced as expected in the region A (conducting fluid) than for the non-conducting fluid (region B).

It arises only for *Ha* >1. The peak velocity is also observed to migrate towards Region-B as the strength of the magnetic field increases, since Region B is non-conducting and experiences less impedance from magnetic effects. The decelerating effect of transverse magnetic field is well known in magnetofluid dynamics owing to the presence of the

Lorentzian hydromagnetic drag force. However when the Lorentzian force exceeds the viscous force in the regime (both forces are of the same order of magnitude when $Ha = 1$), instability arises. To sustain a homogenous retardation in the velocity field across both porous zones A and B, weaker magnetic field is recommended. A similar observation has been reported in purely fluid simulations of MHD channel flow by Lohrasbi and Sahai [46] and for Darcian hydromagnetic flow by Rudraiah *et al*. [47]. This has implications in for example magnetic field control (manipulation) of petroleum flows [48]. It also may be of benefit in newly emerging technologies including de-contamination of coastal and ocean seabeds e.g. magneto-hydrodynamic oil slick (surface spill) control [49]. In the latter the electrically conducting nature of ocean water allows the use of magnetic field to rapidly separate and recover oil from oil-contaminated seawater, using the electromagnetic Lorentz force. This technique avoids the need for mechanical devices and dispersants, and is compact, less noisy and does not damage marine environments, especially seabed ecosystems. The present 2-dimensional simulations also serve as a good benchmark for more complex 3-D models using commercial codes [50].

Fig. 3 depicts the response of the velocity field to a variation in the frequency parameter, εA, *a characteristic* of the lateral mass flux (transpiration) velocity. This parameter when positive implies injection at the upper boundary. It could represent for example mass influx out of a seabed. When negative the case of suction is apparent. With increasing frequency parameter, the flow is accelerated in both regions A and B. A rise in εA corresponds to an increase in amplitude of the periodic oscillations of the transpiration velocity. Such effects are encountered for example in sea-beds owing to the oscillatory nature of wave/current interactions [51]. Greater acceleration is computed in region B. The maximum velocity in the channel is observed to be again in Region B.

Fig. 4 depicts the response of the velocity field to a variation in the periodic frequency parameter, $\omega\tau$. This parameter exerts a significantly less dramatic effect on velocity magnitudes compared with transpiration frequency parameter. However it does have a *weak* accelerating effect on the flow, in particular in region B. It aids in momentum development in particular close to the interface of the two regions.

Fig. 5 depicts the effect of the pressure parameter on the velocity field. With an increase in pressure, the flow is massively decelerated across both regions A and B. The parabolic

profiles at low pressure values are also increasingly flattened as pressure increases. The plateau becomes progressively wider with larger p^*. The inverse relationship between pressure and velocity is clearly highlighted in the profiles. Greater pressure opposes momentum development and retards the flow in both regions.

Figs. 6, 7 illustrate the influence of Darcy numbers on the velocity profiles. Each region has a separate Darcy number, Da_1, Da_2. Forchheimer effects are ignored in fig. 5. These represent the permeabilities of each region. With greater permeability, less solid fibers are present to impede flow. The converse is apparent with lower permeabilities. The Darcy numbers feature respectively in linear Darcian impedance terms in eqns. (8), (9). With a rise in Da_1, Da_2, these drag forces are reduced. This accelerates the flow in the two regions. For the case when both regions have the same Darcy number, $Da_1 = Da_2 = 0.01$, the velocities are minimized, since these low permeabilities imply a very strong Darcian impedance. For the case where $Da_1 > Da_2$, the velocity is significantly elevated in region A compared with region B. The contrary effect is witnessed when $Da_1 < Da_2$, for which region B is more permeable than region A. **Fig. 7** shows similar trends to Fig. 6 with larger values of Darcy numbers. The decelerating nature of lower permeabilities in regulating flow is therefore clearly established.

Figs. 8, 9 illustrate the influence of Forchheimer numbers on velocity distributions. As with Darcy number, a separate Forchheimer number, Fs_1, Fs_2. Forchheimer effects are associated with a second order (inertial) drag which becomes dominant at higher velocities. Unlike Darcy number, which has an inverse relationship with Darcian impedance forces, Forchheimer drag effects are directly proportional to Forchheimer numbers. As Fs_1, *is increased,* Forchheimer drag forces are accentuated. This leads to a retardation in the flow, as observed in fig. 8, where Fs_2 *is* fixed. The greater decrease in velocity in region A is associated with the growing Forchheimer impedance in region A, whereas that in region B is unaltered. The contrary effect is observed in fig 9, where the Forchheimer drag in region A is unchanged, and a strong increase enforced in region B leading to the significantly lower velocities in region B.

Fig. 10 illustrates the effects of viscosity ratio parameter, $\alpha = \frac{\mu_2}{\mu_1}$, on velocity profiles in region A and region B. With greater viscosity ratio, there is an evident deceleration in the

flow in both regions. Greater viscosity implies greater viscous drag force. This retards momentum development. There is a more prominent deceleration in region A, since a greater viscosity arises here than in region B.

Fig. 11 finally shows the effect of the transpiration velocity, v_o, on velocity evolution in regions A and B. With greater transpiration effect, the flow is strongly accelerated in both regions. The momentum is boosted with injection of fluid, and the effect is greatest in region B.

7. Conclusions

A mathematical model has been developed for the two-immiscible fluid flow in a dual porous medium with an interface between the fluids in the presence of a transverse magnetic field. The Navier-Stokes equations have been reduced to a dimensionless pair of second order partial differential equations coupled via a common oscillatory y^*-direction velocity and a fluid viscosity ratio. A number of special cases of the model have been presented. Two numerical methods, viz the finite difference method and a finite element method are used to solve the dimensionless boundary value problem subject to appropriate hydrodynamic boundary and interfacial conditions. Very good correlation has been achieved between the two methods. Computations have shown that increasing Hartmann number significantly decelerates the flow in region A, whereas increasing Darcy number (porous medium permeability) accelerates the flow in both regions. Increasing Forchheimer number retards flow in both regions. With greater viscosity ratio, the flow is decelerated in both regions. The present model is relevant to new technologies utilizing magnetohydrodynamic control of oil separation in contaminated geological zones.

References

[1] Packham, B.A. and Shail,R., Stratified laminar flow of two immiscible fluids, *Proc. Cambr. Phil. Soc.*, 69, 443-448 (1971).

[2] Ranger, K.B., The two-phase Stokes flow of two immiscible fluids, *Technical Report, Mathematics Research Center, Wisconsin University, Madison, USA, January* (1973).

[3] Napolitano, N.G., Plane Marangoni-Poiseuille flow of two immiscible fluids, *30th Int. Astronautical Congress, Munich, West Germany, September 17-22* (1979).

[4] Than, P.T., Rosso, F. and Joseph, D.D., Instability of Poiseuille flow of two immiscible liquids with different viscosities in a channel, *Int. J. Engineering Science*, 25, 2, 189-204 (1987).

[5] M.-E.M. Khedr, A.J. Chamkha, M. Bayomi, MHD flow of a micropolar fluid past a stretched permeable surface with heat generation or absorption, *Nonlinear Analysis: Modelling and Control*, Vol. 14, No. 1, 27-40, 2009.

[6] A. J. Chamkha, MHD-free convection from a vertical plate embedded in a thermally stratified porous medium with Hall effects, *Applied Mathematical Modelling*, Vol. 21, Issue 10, pp.603-609, 1997.

[7] E. Magyari, A.J. Chamkha, Exact analytical results for the thermosolutal MHD Marangoni boundary layers, *Int. J. Thermal Sciences*, 47, 848-857, 2008.

[8] Ali. J. Chamkha, Ali Al-Mudhaf, Unsteady heat and mass transfer from a rotating vertical cone with a magnetic field and heat generation or absorption effects, *Int. J. Thermal Sciences*, Vol. 44, Issue 3, pp.267-276, 2005.

[9] Ali. J. Chamkha, Abdul-Rahim A. Khaled, Similarity solutions for hydromagnetic mixed convection heat and mass transfer for Hiemenz flow through porous media, *Int. J. Numerical Methods for Heat & Fluid Flow*, Vol. 10, No. 1, pp.94-115, 2000.

[10] Ali. J. Chamkha, Unsteady laminar hydromagnetic fluid-particle flow and heat transfer in channels and circular pipes, Int. J. Heat and Fluid Flow, Vol. 21, pp.740-746, 2000.

[11] Shail, R., On laminar two-phase flow in magnetohydrodynamics, *Int. J. Engineering Science*, 11, 10, 1103-1108 (1973).

[12] Baier, G. and Graham, M.D., Two-fluid Taylor Couette flow: experiments and linear theory for immiscible liquids between co-rotating cylinders, *Physics of Fluids*, 10, 12, 3045-3055 (1998).

[13] Adler, P.M., *Porous Media: Geometry and Transport*, Butterworths, USA (1993).

[14] Bear, J. and Verruijt, A., *Modeling Groundwater Flow and Pollution*, Dordrecht, Netherlands (1987).

[15] Hong, J.T., Tien, C.L. and Kaviany, M., Non-Darcian effects on vertical plate natural convection in porous media with high porosities, *Int. J. Heat Mass Transfer*, 28, 2149-2157 (1985).

[16] O. Anwar Bég, R. Bhargava, S. Rawat, H. S. Takhar, M. Kalim Halim, Computational modeling of biomagnetic micropolar blood flow and heat transfer in a two-dimensional non-Darcian porous medium, *Meccanica,* 43, 4, 391-410 (2008).

[17] O. Anwar Bég, J. Zueco, R. Bhargava, H.S. Takhar, Magnetohydrodynamic convection flow from a sphere to a non-Darcian porous medium with heat generation or absorption effects: network simulation, *Int. J. Thermal Sciences*, 48, 5, 913-921 (2009).

[18] J. Zueco, O. Anwar Bég and S.K. Ghosh, Unsteady natural convection of a short-memory viscoelastic fluid in a non-Darcian regime: network simulation, *Chemical Engineering Communications*, 198, 172-190 (2010).

[19] M.M. Rashidi, M. Keimanesh, O. Anwar Bég and T.K. Hung, Magneto-hydrodynamic biorheological transport phenomena in a porous medium: A simulation of magnetic blood flow control and filtration, *Int. J. Numerical Methods in Biomedical Engineering*, 27, 805–821 (2011).

[20] O. Anwar Bég, Tasveer A. Bég, R. Bhargava, S. Rawat and D. Tripathi, Finite element study of pulsatile magneto-hemodynamic non-Newtonian flow and drug diffusion in a porous medium channel, *J. Mechanics in Medicine and Biology,* 12 (4) 1250081.1 – 1250081.26 (2012).

[21] G. Swapna, L. Kumar, O. Anwar Bég and B. Singh, Finite element analysis of radiative mixed convection magneto-micropolar flow in a Darcian porous medium with variable viscosity and convective surface condition, *Heat Transfer- Asian Research,* 1–18 (2014). **DOI 10.1002/htj.21134**

[22] O. Anwar Bég, M. S. Khan, I. Karim, M. M. Alam, M. Ferdows, Explicit numerical simulation of magnetohydrodynamic nanofluid flow from an exponential stretching sheet in porous media, *Applied Nanoscience,* 4, 943-957 (2014).

[23] O. Anwar Bég, S. Rawat, J. Zueco, L.Osmond and R.S.R.Gorla, Finite element and network electrical simulation of rotating magnetofluid flow in nonlinear porous media with inclined magnetic field and Hall currents, *Theor. Appl. Mech.,* 41, (1), 1–35 (2014).

[24] Lennon, G.P., Three dimensional simulation of two-fluid movement in porous media using the boundary element method, *Hydraulics and Hydrology in the Small Computer Age, ASCE Spec. Conference, W.R. Waldrop (Editor)*, 474-479, New York, USA (1985).

[25] DeGregoria, A.J., Monte Carlo simulation of two-fluid flow through porous media at finite mobility ratio- the behaviour of cumulative recovery, *Physics of Fluids*, 29, 11, 3557-3561 (1986).

[26] Casulli, V. and Greenspan, D., Numerical simulation of miscible and immiscible fluid flows in porous media, *AIME Soc. Petroleum Engineers J*., 22, 635-646 (1982).

[27] Than, P.T., Rosso, F. and Joseph, D.D., Instability of Poiseuille flow of two immiscible fluids with different viscosities in a channel, *Int. J. Engineering Science*, 25, 2, 189-204 (1987).

[28] Chamkha, A.J., Flow of two immiscible fluids in porous and non-porous channels, *ASME J. Fluids Engineering*, 122, 1, 117-124 (2000).

[29] Y. Peng *et al*., Experimental study on MHD oil separation from oil-contaminated seawater using high field superconducting magnet, *Int. J. Offshore Polar Engineering*, 17, 189–192 (2007).

[30] Lohrasbi, J. and Sahai, V., Magnetohydrodynamic heat transfer in two phase flow between parallel plates, *Appl. Sci. Research*, 45, 53-66 (1987).

[31] Umavathi, J.C., Mateen, A., Chamkha, A.J. and Al-Mudhaf, A., Oscillatory Hartmann two-fluid flow and heat transfer in a horizontal channel, *Int. J. Applied Mechanics Engineering*, 11, 1, 155-178 (2006).

[32] N. Ali, A. Zaman and O. Anwar Bég, Unsteady magnetohydrodynamic blood flow in a porous-saturated overlapping stenotic artery: Numerical modelling, *J. Mechanics in Medicine and Biology*, 16, 1650049.1-1650049.16 (2016).

[33] K.A. Hoffmann and S.T. Chaing, *Computational Fluid Dynamics*, Vol. 1, Fourth Edition, *Engineering Education System*, New York, USA (2000).

[34] N. Ali, K. Javid, M. Sajid and O. Anwar Bég, Numerical simulation of peristaltic flow of a biorheological fluid with shear-dependent viscosity in a curved channel, *Computer Methods in Biomechanics and Biomedical Engineering*, 19 (6) 614-627 (2016).

[35] Nasir Ali, Akbar Zaman and O. Anwar Bég, Numerical simulation of unsteady micropolar hemodynamics in a tapered catheterized artery with a combination of stenosis and aneurysm, *Medical and Biological Engineering and Computing*, 54, 1423–1436 (2016).

[36] A. Zaman, N. Ali, O. Anwar Bég and M. Sajid, Heat and mass transfer to blood flowing through a tapered overlapping stenosed artery, *Int. J. Heat Mass Transfer,* 95, 1084-1095 (2016).

[37] O. Anwar Bég, N. Ali, A. Zaman, Eemaan T. A. Bég and Ayesha Sohail, Computational modelling of heat transfer in annular porous medium solar energy absorber with a P1-radiative differential approximation, *J. Taiwan Inst. Chemical Eng.,* 66, 258-268 (2016).

[38] Nasir Ali, Akbar Zaman, O. Anwar Bég, M.Sajid, Unsteady two-layer blood flow through a *w*-shape stenosed artery using the generalized Oldroyd-B fluid model, *ANZIAM Journal,* 58, 1-23 (2016). doi:10.1017/S1446181116000134

[39] D. Gupta, Lokendra Kumar, O. Anwar Bég and B. Singh, Finite element simulation of mixed convection flow of micropolar fluid over a shrinking sheet with thermal radiation, *Proc IMechE- Part E: J. Process Mechanical Engineering***,** 228 (1), 61-72, (2014).

[40] O. Anwar Bég, R. Bhargava, S. Singh and H. Maregere, Element-Free Galerkin method (EFGM) computation of transient micropolar magnetic squeeze film flow, *Int. J. Applied Mathematics and Mechanics,* 16, 1-21 (2013).

[41] P. Rana, R. Bhargava and O. Anwar Bég, Finite element simulation of unsteady MHD transport phenomena on a stretching sheet in a rotating nanofluid, *Proc. IMECHE- Part N; J. Nanoengineering and Nanosystems,* 227, 77-99 (2013).

[42] D. Gupta, L. Kumar, O. Anwar Bég, B. Singh, Finite element analysis of transient heat and mass transfer in microstructural boundary layer flow from porous stretching sheet, *Comp. Thermal Sci. 6 (2),* 155-169 (2014).

[43] V. Rajesh, O. Anwar Beg, Ch. Sridevi and K. Jonah Phillip, Finite element analysis of unsteady MHD free convective laminar boundary-layer accelerated dissipative flow with uniform suction and chemical reaction, *Int. J. Energy & Technology*, 6, 1-10 (2014).

[44] J.L. Curiel Sosa, O. Anwar Bég and J.M. Liebana Murillo, Finite element analysis of structural instability using a switching implicit–explicit technique, *Int. J. Computational Methods in Engineering Science and Mechanics,* 14, 452-464 (2013).

[45] O. Anwar Bég, Numerical methods for multi-physical magnetohydrodynamics, Chapter 1, pp. 1-112, *New Developments in Hydrodynamics Research, Nova Science, New York, September* (2012).

[46] Lohrasbi J. and Sahai V., Magnetohydrodynamic heat transfer in two phase flow between parallel plates, *Appl. Sci. Res*., 45, 53-66 (1987).

[47] Rudraiah N., Ramaih B.K. and Rajashekhar B.M., Hartmann flow over a permeable bed, *Int. J. Eng. Sci*., 13, 1-24 (1975).

[48] Ivakhnenko, O.P., Magnetic analysis of petroleum reservoir fluids, matrix mineral assemblages and fluid-rock interaction. *PhD Thesis, Heriot-Watt University, Institute of Petroleum Engineering, Edinburgh*, UK (2006).

[49] P. Yan, Z. Lingzhi, L. Ran, S. Ciwen and X. Yuyu, Experimental and analytical study on MHD oil-spill recovery from oil-contaminated seawater, *7th Pacific/Asia Offshore Mechanics Symposium, Dalian, China, September 17–20* (2006).

[50] C. Ye, L.Z. Zhao, Y.J. Liu, 3D numerical analysis on flow process of floating-oil recovery device by MHD method, *23RD International Offshore and Polar Engineering Conference, 30 June-5 July, Anchorage, Alaska* (2013).

[51] J. F. A. Sleath, *Seabed Mechanics*, Wiley, USA (1984).

TABLES

y	*Velocity (u_1 * =u_2*)*					
	$\alpha = 0.25$ FTCS	$\alpha = 0.25$ MAGNETO-FEM	$\alpha = 0.5$ FTCS	$\alpha = 0.5$ MAGNETO-FEM	$\alpha = 3$ FTCS	$\alpha = 3$ MAGNETO-FEM
-1.0000	0	0	0	0		0
-0.8000	0.2301	0.2302	0.2024	0.2022	0.1186	0.1187
-0.6000	0.3348	0.3347	0.3079	0.3076	0.2016	0.2017
-0.4000	0.3802	0.3804	0.3603	0.3601	0.2573	0.2574
-0.2000	0.3981	0.3979	0.3817	0.3815	0.2912	0.2911
0	0.3850	0.3852	0.3699	0.3672	0.3062	0.3063
0.2000	0.3508	0.3503	0.3428	0.3429	0.3093	0.3095
0.4000	0.3258	0.3259	0.3216	0.3217	0.3039	0.3038
0.6000	0.2920	0.2921	0.2898	0.2897	0.2807	0.2808
0.8000	0.2140	0.2141	0.2130	0.2131	0.2088	0.2086
1.0000	0	0	0	0	0	0

Table 1: Velocity evolution across the channel for different values of α

FIGURES

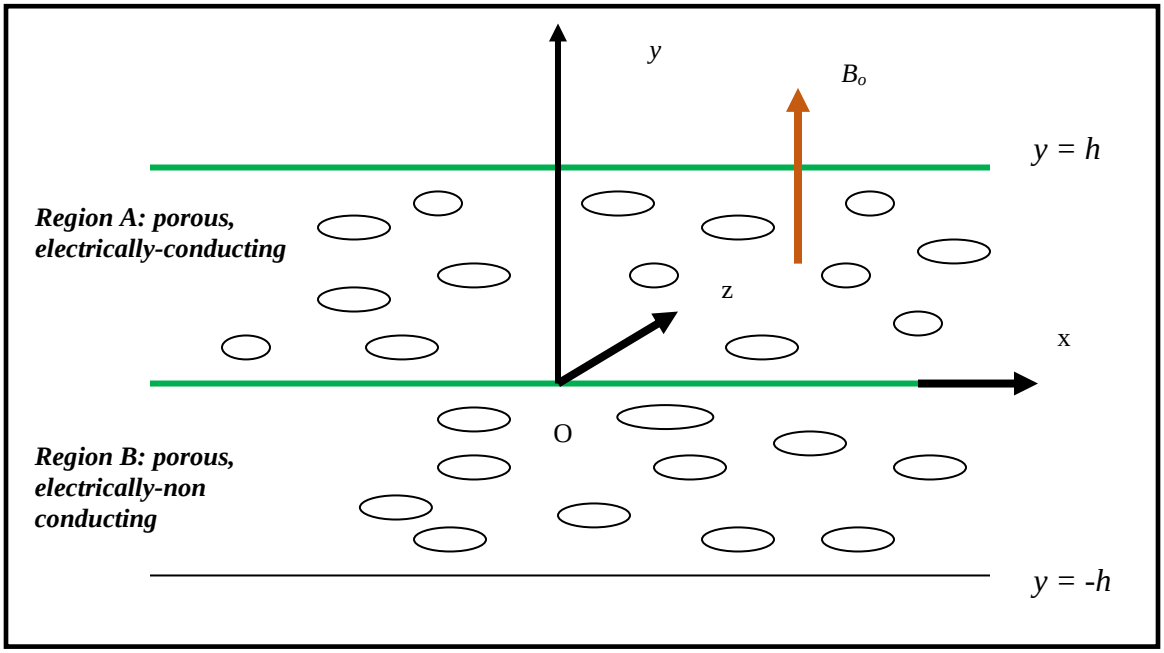

Figure 1: Physical Model and Coordinate System

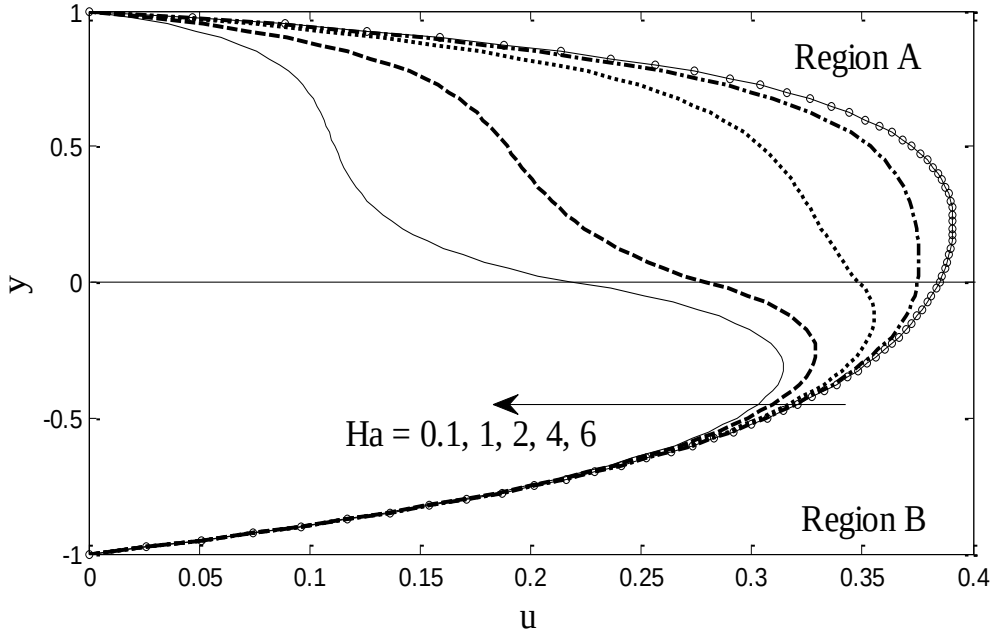

Fig 2: y versus u i.e. u_1 * and u_2 * (both region A and B) for various Ha.

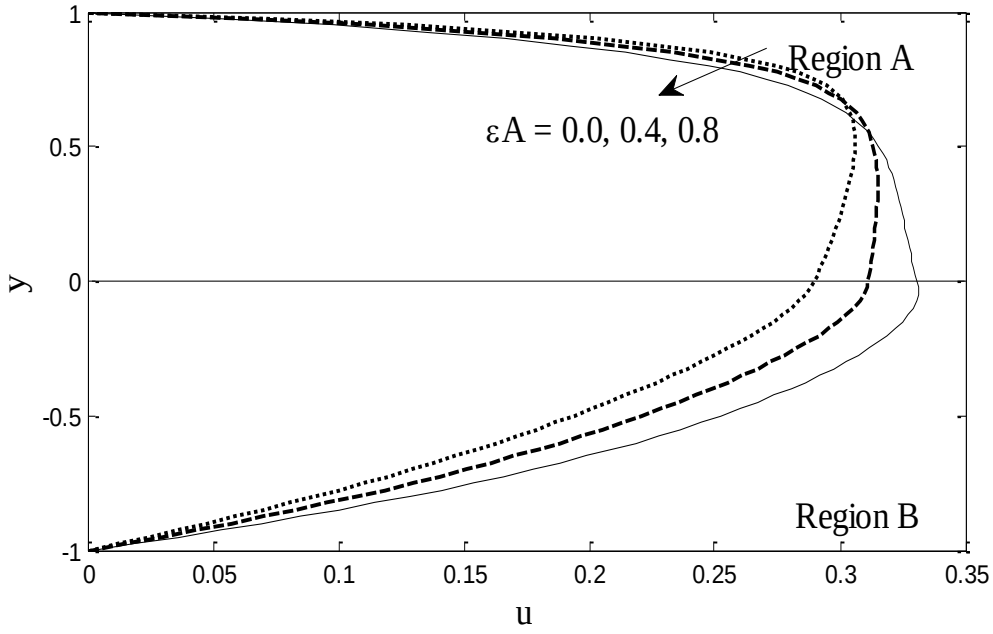

Fig 3. y versus u i.e. u_1 * and u_2 * (both region A and B) for various εA.

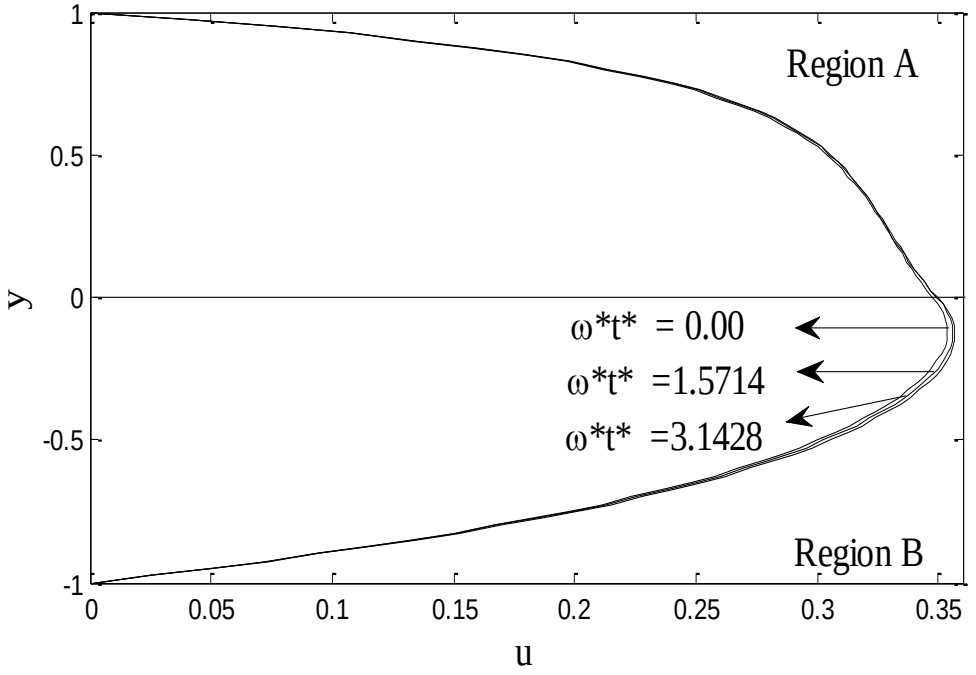

Fig. 4. y versus u i.e. u_1 * and u_2 * (both region A and B) for various ω^*t^*.

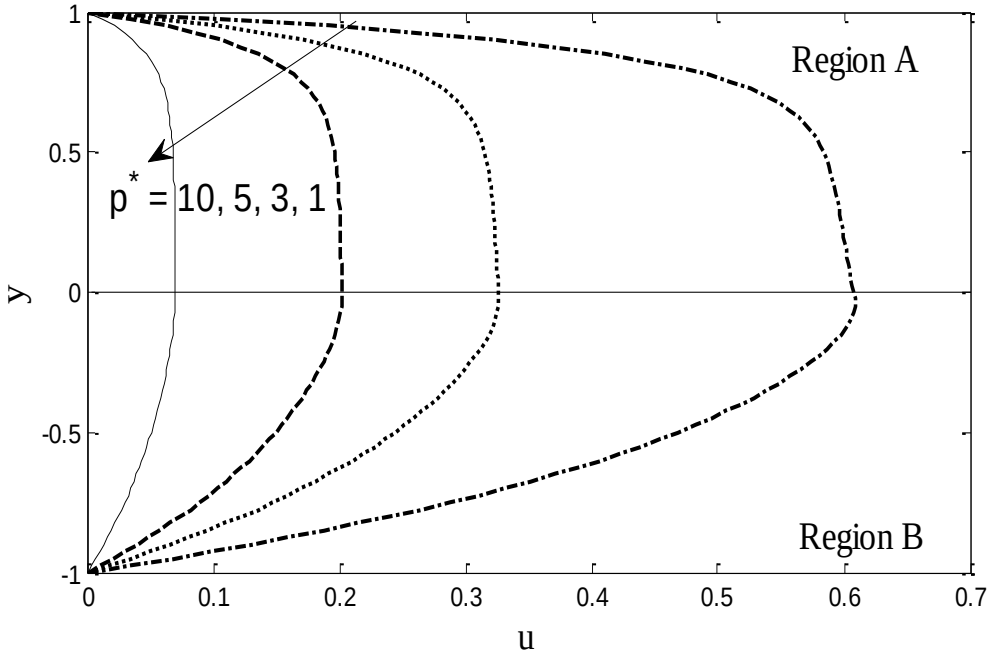

Fig. 5. y versus u i.e. u_1 * and u_2 * (both region A and B) for various p*.

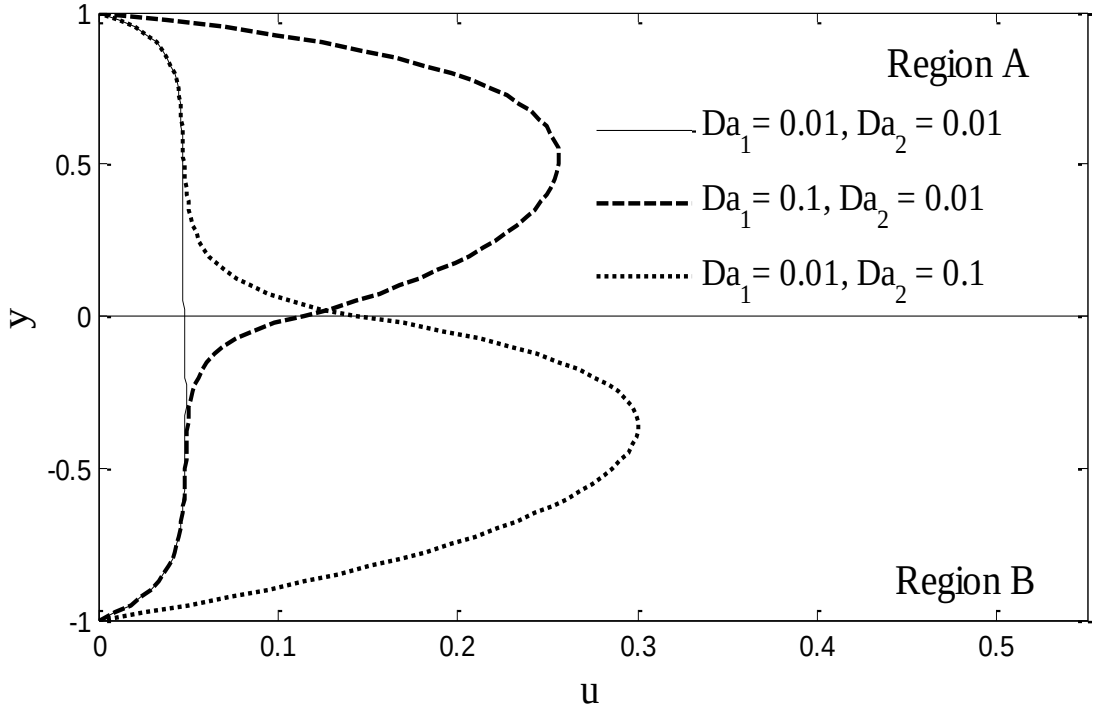

Fig. 6. y versus u i.e. u_1 * and u_2 * (both region A and B) for various Da_1, Da_2 [Darcy numbers for region A and region B] - *for Darcian case only* i.e. $Fs_1 = Fs_2 = 0$.

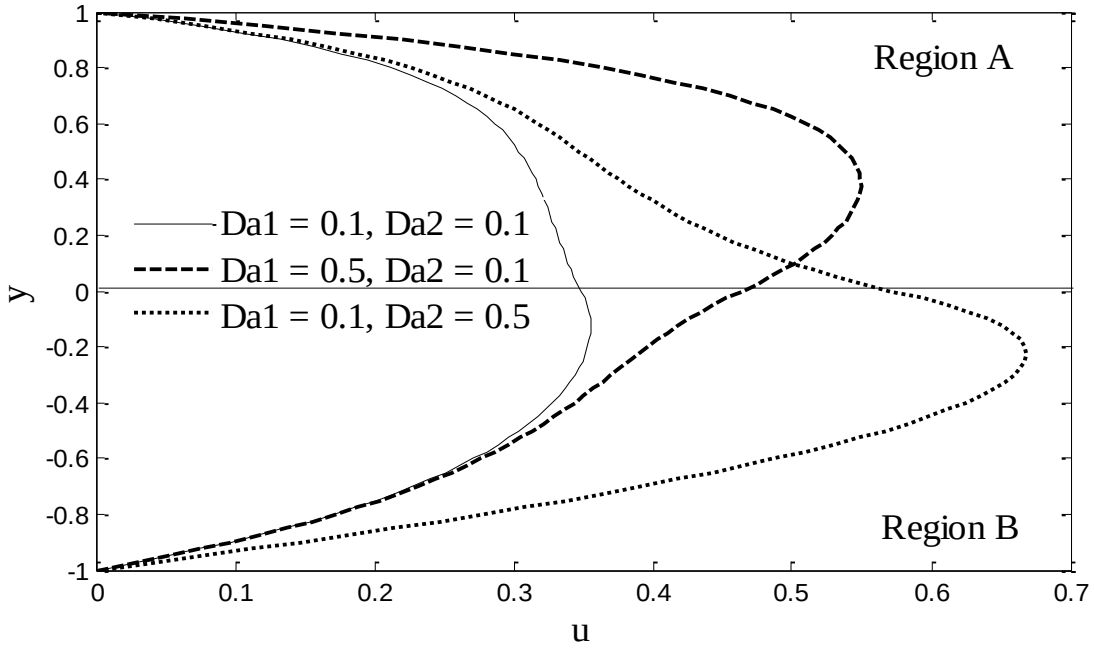

Fig. 7. y versus u i.e. u_1 * and u_2 * (both region A and B) for various Da_1, Da_2 [Darcy numbers for region A and region B] - *for Darcian case only* i.e. $Fs_1 = Fs_2 = 0$.

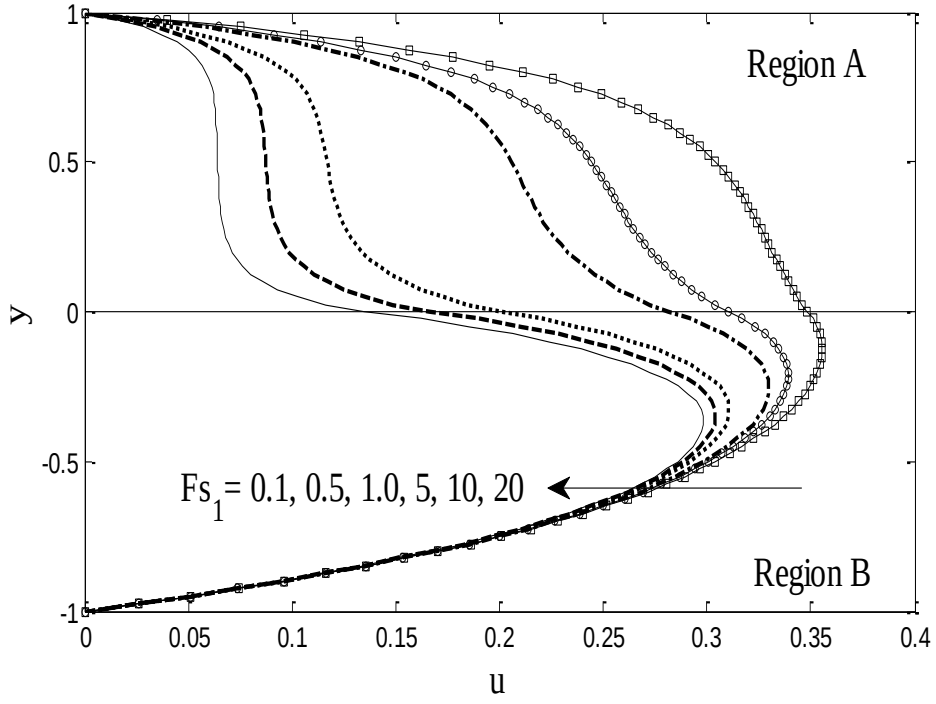

Fig. 8. y versus u i.e. u_1 * and u_2 * (both region A and B) for various Fs_1 variation with Fs_2 fixed at 0.1 [Darcy numbers for region A and region B = 0.001 each].

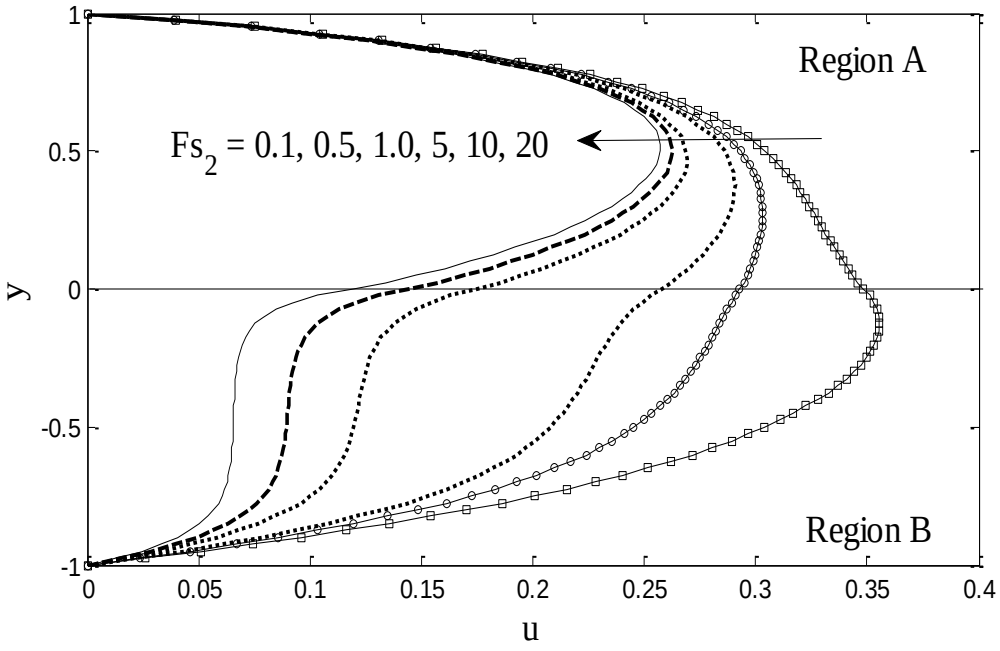

Fig. 9 y versus u i.e. u_1* and u_2* (both region A and B) for various Fs_2 variation with Fs_1 fixed at 0.1 [Darcy numbers for region A and region B=0.001 each].

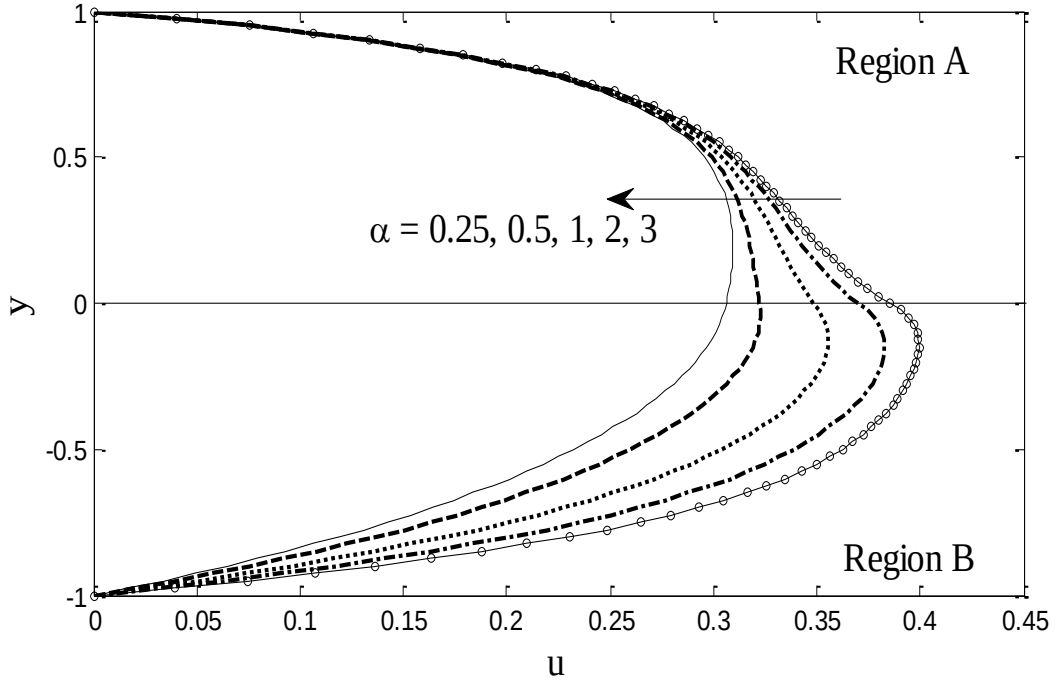

Fig. 10. y versus u i.e. u_1 * and u_2 * (both region A and B) for various α.

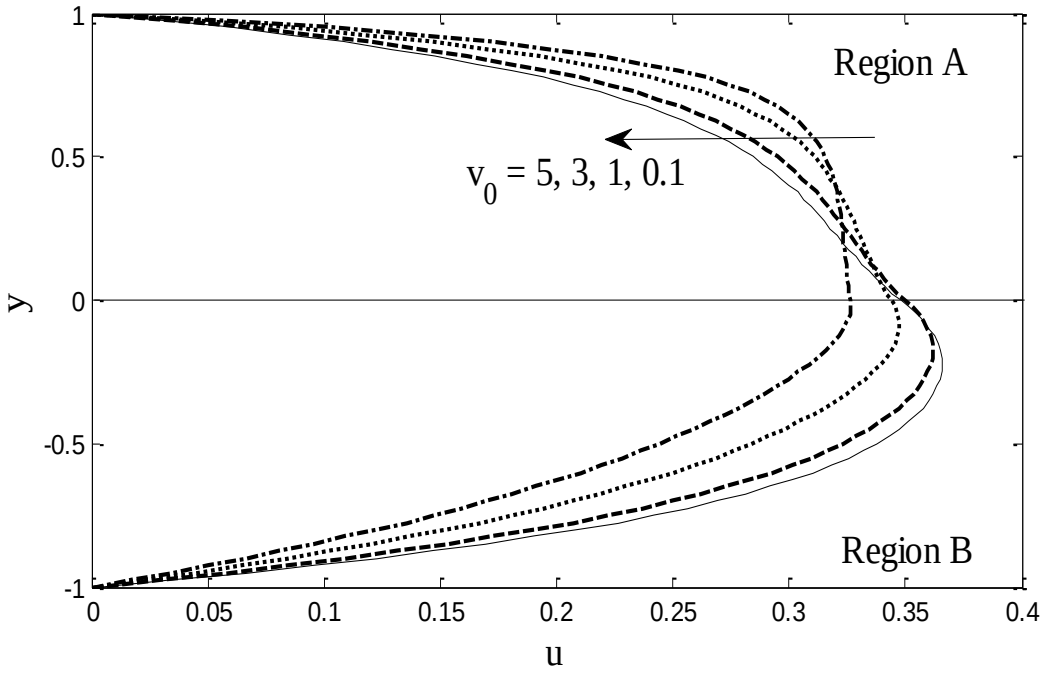

Fig. 11. y versus u i.e. u_1 * and u_2 * (both region A and B) for various v_0 .